

Current Biology, Volume 23

Supplemental Information

Quantitative Imaging of Transcription

in Living *Drosophila* Embryos Links

Polymerase Activity to Patterning

Hernan G. Garcia, Mikhail Tikhonov, Albert Lin, and Thomas Gregor

SUPPLEMENTAL EXPERIMENTAL PROCEDURES

Cloning of transgenes

A pUC18 vector containing the construct pNOS-NLS-MCP-eGFP- α Tub3'UTR was kindly provided by Liz Gavis (Princeton University). This construct contains the MS2 coat protein (MCP) fused to eGFP under the control of the *nanos* promoter. It bears a nuclear localization signal (NLS) and an α Tubulin 3'UTR. The NLS was removed by amplifying the plasmid with primers 2.14 and 2.15. The resulting plasmid pUC18-pNOS-NLS-MCP-eGFP- α Tub3'UTR was then inserted into pCASPER4 using the KpnI and HpaI sites for P-element transgenesis. NLS-MCP-GFP has been reported to localize in puncta within nuclei even in the absence of reporter in the early embryo [S1]. This artifact could be completely abolished by removing the nuclear localization signal from MCP-GFP while still maintaining significant protein levels within nuclei. 12 copies of the stem loops were extracted from plasmid pSL-MS2-12X (Addgene 27119) by digesting with PstI and EcoRV. This fragment was ligated back into pSL-MS2-12X digested with EcoRV in order to create pSL-MS2-24X. Plasmid piB-hbP2-P2P-lacZ- α Tub3'UTR was kindly provided by Steve Small (NYU) [S2]. It contains the *hunchback* P2 enhancer and promoter driving the *lacZ* gene fused to an α Tubulin 3'UTR. This sequence is flanked by attB sites, which can be used for recombinase-mediated cassette exchange (RMCE) into the fly genome at specific landing sites [S3]. In order to insert the MS2 stem loops into this reporter construct unique restriction sites were created either at the 5' or 3' of the *lacZ* gene using site-directed mutagenesis (Quikchange II; Stratagene). For the 5' construct NcoI and AvrII sites were created using primer 1.12. This plasmid was digested using the two new restriction enzymes and combined with an NcoI-AvrII fragment from pSL-MS2-24X in order to create piB-hbP2-P2P-MS2-24x-lacZ- α Tub3'UTR.

Primer name and number	Sequence	Description
2.14-Pnos-NoNLS-CCW	tattatatgcatgatctatggaaaatccgggtcg	Amplify the pUC18-pNOS-NLS-MCP-eGFP- α Tub3'UTR plasmid while deleting the NLS and inserting an NsiI site
2.15-Pnos-NoNLS-CW	attataatgcatcaccatggcttctaactttactcagttcgtt	
1.12-P2PupV2-NcoI-NsiI	cgtctagagccgccaagtacccatggctatcacaatgcatatgcagaactgggagacgac	Create NcoI and AvrII sites at the 5' end of the <i>lacZ</i> gene in piB-hbP2-P2P-lacZ- α Tub3'UTR
1.5-P2PlacZdw-NcoI-NsiI	gtctggtgtcaaaaataaccatggctatcacaaatgcattaataaccggggcagg	Create NcoI and NsiI sites at the 3' end of the <i>lacZ</i> gene in piB-hbP2-P2P-lacZ- α Tub3'UTR

For the 3' construct, NcoI and NsiI sites were created using primer 1.5. Here, the plasmid was digested with the new restriction sites and ligated with a fragment obtained from pSL-MS2-24X using the same restriction enzymes in order to create piB-hbP2-P2P-lacZ-MS2-24x- α Tub3'UTR. The resulting geometry of our reporter constructs is such that polymerases in the 5' construct transcribe through the 1336bp long MS2 region and through 3960bp more DNA until reaching the end of the transcript, while in the 3' construct transcription continues only through 605bp after the loops. All steps were confirmed by sequencing. Plasmids and plasmid sequences are available upon request.

Fly strains and genetics

The construct pCASPER4-pNOS-MCP-eGFP- α Tub3'UTR was randomly inserted into the fly genome using P-element transgenesis (BestGene). Several clones were isolated. For this particular work, a line on the III chromosome, called *MCP-NoNLS(2)*, was established. A *Histone-RFP* fusion (*His2Av-mRFP1*, FBti0077845) on the second chromosome was used to create the fly line *yw;Histone-RFP;MCP-NoNLS(2)*. Line *Bcd-GFP;Histone-RFP;Bcd^{E1}* for the measurements shown in Figure S1C was generated from lines *Bcd-GFP;Bcd^{E1}* [S4] and *Histone-RFP*. To determine the activity of our

reporter in the absence of Bcd activator the *Bcd^{E1}* and *MCP-GFP* lines were recombined to create *yw;Histone-RFP;Bcd^{E1},MCP-NoNLS(2)*. Constructs piB-hbP2-P2P-MS2-24x-lacZ- α Tub3'UT and piB-hbP2-P2P-lacZ-MS2-24x- α Tub3'UTR were inserted into the fly genome using the RMCE approach [S3] to create fly lines *P2P-MS2-lacZ* and *P2P-lacZ-MS2*, respectively.

Sample preparation and data acquisition

Female virgins of line *yw;Histone-RFP;MCP-NoNLS(2)* or of *yw;Histone-RFP;Bcd^{E1},MCP-NoNLS(2)* were crossed with males of the reporter line (*P2P-MS2-lacZ* or *P2P-lacZ-MS2*). Collected embryos were dechorinated and mounted between a semipermeable membrane (Biofolie, In Vitro Systems & Services) and a coverslip and embedded in Halocarbon 27 oil (Sigma). Excess oil was removed with absorbent paper from the sides in order to flatten the embryos slightly. The flattening of the embryos makes it possible to image more nuclei in the same focal plane without causing any detectable change to early development processes [S5]. Embryos were imaged using a custom-built two-photon microscope [S6] with a laser wavelength of 970 nm to excite both MCP-GFP and Histone-RFP. Fluorescence was collected with two separate photomultiplier tubes (gallium-arsenide-phosphide photomultiplier tube, module H10770PA-40 SEL Hamamatsu). Pixel size is 220 nm and image resolutions are 512x256 pixels or 128x128 pixels. At each time point a stack of 10 images separated by 1 μ m was acquired. For each slice of the stack three individual images were taken, aligned and averaged offline. The final time resolution is 37s (512x256 window) and 10s (128x128 window), respectively.

Live imaging data analysis

Histone-RFP slices were maximum projected for each time point. Nuclei were segmented using available segmentation software optimized for *Drosophila* early embryonic development [S7]. The segmented nuclei were then tracked over multiple nuclear cycles by adapting an available code [S8]. Initially, each time frame of the MCP-GFP channel is treated independently. Spots are detected in 3D using raw images [S9, 10] (Figure S2I) and assigned to their respectively closest nucleus. When multiple spots are detected in the vicinity of the nucleus (due to segregating sister chromatids) only the brightest one is kept. When single traces are shown, the automated tracking of both nuclei and spots was checked manually frame by frame using custom analysis code. Spot intensity determination requires an estimate of the local fluorescent background for each particle. 2D Gaussian fits to the peak plane of each particle column (Figure S2I) determines an offset, which is used as background estimator. The intensity is calculated by integrating the particle fluorescence over a circle with a radius of 6 pixels and subtracting the estimated background. Imaging error is dominated by the error made in the fluorescent background estimation (Figure S2C-G).

Single molecule mRNA FISH sample preparation and data analysis

Single molecule mRNA FISH was performed as previously described [S9, 10]. Probes against the *lacZ* gene were functionalized with Atto565 dye. To avoid degradation of endogenous GFP fluorescence, methanol washed and incubations in the FISH protocol [S9, 10] were sped up as much as possible. Data was analyzed as described in [S9].

SUPPLEMENTAL FIGURES

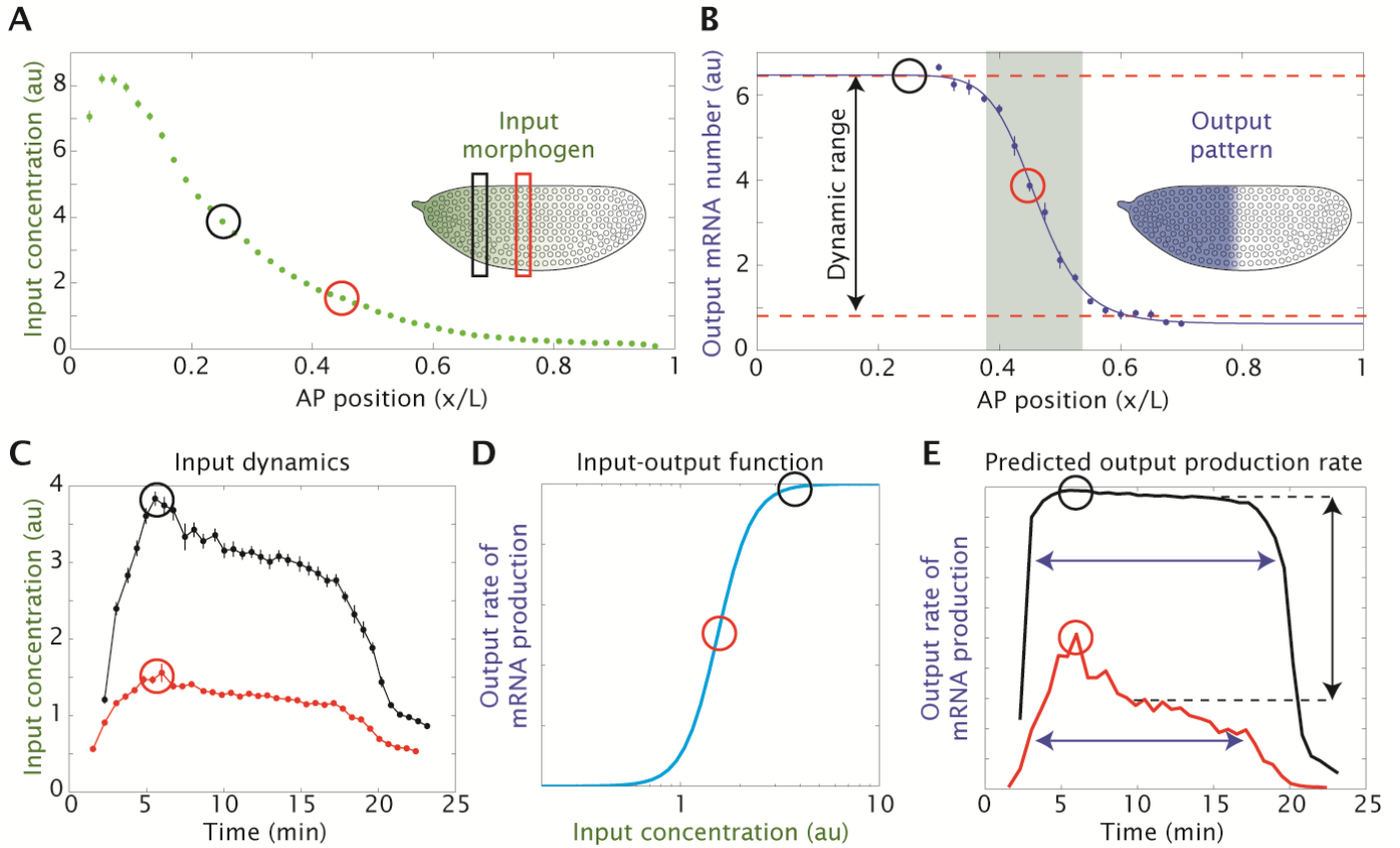


Figure S1. Dynamic developmental pattern formation, related to Figures 1 and 3. (A-B) A space-varying input morphogen (A, data shown for Bcd-GFP [S6]) determines an output pattern of accumulation of its target gene (B, measured by counting accumulated transcripts). The dynamic range and transition region (shaded area) of the boundary are shown. Black and red circles indicate measurements in nuclei in the anterior and in the transition regions of the profile throughout the figure, respectively. (C) The nuclear concentration of the Bcd input morphogen is subject to spatial modulation as in (A) and, in addition, to temporal modulation throughout the nuclear cycle (colors indicate nuclear averages at two positions in the embryo (see (A))). (D) An input-output function has been hypothesized to determine the output *rate of mRNA production* as a function of the instantaneous input concentration of transcription factor [S11-14]. (E) The input-output function in (D) coupled with the input dynamics in (C) predicts the modulation of the average rate of mRNA production of the output gene (black arrow) and of the window of time over which transcription ensues (blue arrows). (A, error bars are standard errors over multiple embryos; B,C, error bars are standard errors over multiple nuclei).

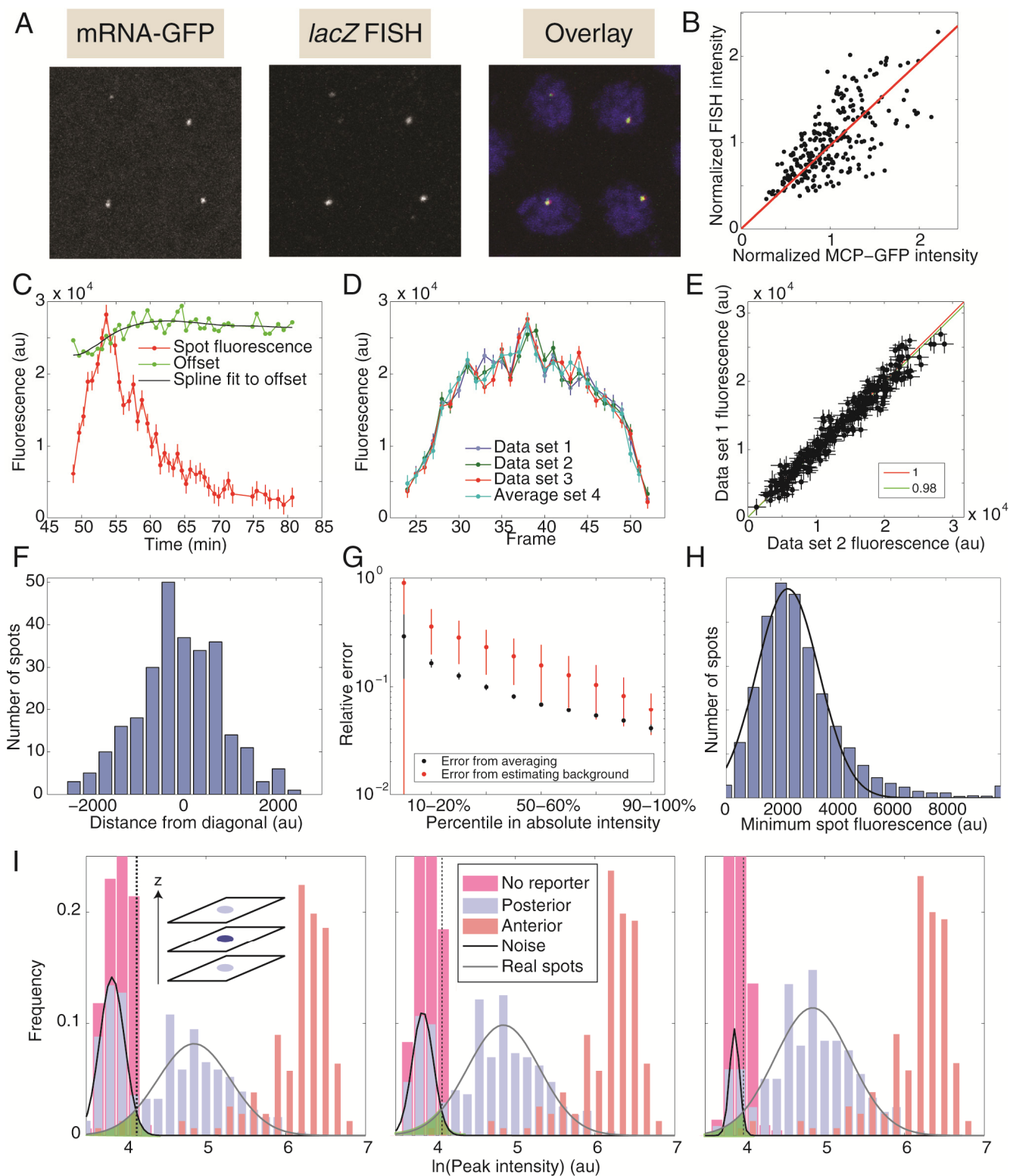


Figure S2. Spot detection and fluorescence measurement, related to Figure 2. (A) MCP-GFP spots are related to sites of nascent transcripts. Embryos were fixed during interphases 13 and 14 and stained using oligonucleotide probes against *lacZ* mRNA. Fluorescent spots in the *lacZ* FISH channel have been previously shown to be sites of nascent transcripts [S9, 15]. A strong co-localization between these spots and spots of preserved endogenous GFP expression in the MCP-GFP channel is observed (larger than 90%, $n=2$). Images are $15\mu\text{m} \times 15\mu\text{m}$. Extra spots in the *lacZ* FISH channel correspond to finished individual mRNA transcripts that cannot be resolved in the MS2 channel or to sites of nascent transcription with a load of

RNAP below the detection limit. Overlay shows MCP-GFP (green), *lacZ* FISH (red) and DAPI (blue) channels. **(B)** The spot intensities in the MCP-GFP channel correlate with the corresponding intensities of nascent transcription spots in the FISH channel, which had previously been shown to be a measure of the number of actively transcribing PolII molecules [S9]. Intensities in both channels are normalized to their means. Red line is a linear fit with zero y-intercept. The large spread of the data is a signature of the stochastic RNAP distributions along the gene. FISH probes are distributed along the length of the mRNA, and therefore their intensities report on the total length of nascent mRNA at a site of transcription. Polymerases will appear brighter the closer they are to 3' end of the transcript. A given number of polymerases can therefore give rise to a range of possible intensities. **(C, left inset)** A Difference-of-Gaussian (DoG) filter is applied to all planes imaged at a given time point [S9, 10]. This filter maximizes the contrast in each image. Spots found in at least three consecutive planes are combined into a column. Spots that cannot fulfill this requirement are rejected. A second selection occurs by thresholding on the DoG value of the shadow plane. The third selection corresponds to only assigning one spot per nucleus. When multiple spots are found in the vicinity of a nucleus the brightest one is kept. Finally, the resulting distribution of DoG values in the peak plane is explored. **(C)** Typical spot trace and fluorescent offset signal as a function of time in the anterior region in n.c. 14. A 2D Gaussian fit to each particle at every time point is performed in order to estimate the fluorescent background (green). The resulting background as a function of time is fitted to a spline (black line). Spot intensity is calculated by integrating the particle fluorescence over a circle with a radius of 6 pixels and subtracting the background estimated from the spline at each time point (red). The standard deviation of the offset of the data around this spline is used to determine the imaging error associated with each particle. The errors in offset and particle fluorescence measurements are assumed to be comparable and uncorrelated. Hence the error in spot fluorescence is approximated by the offset error times $\sqrt{2}$. **(D-G)** To estimate the imaging noise, fluorescent traces are taken at a frame rate four times higher than our standard protocol while maintaining the same exposure and assembled into four different data sets of the same embryo. **(D)** Fluorescence as a function of frame number for the same spot as measured using the different data set sets shows that the traces are comparable. **(E)** Fluorescence of each spot at each time point in data set 1 as a function of the corresponding fluorescence in data set 2. Red line has a slope of one and green line is a linear fit with a slope of 0.98. This fit is performed for all combinations of data sets to obtain an average slope of 0.99 ± 0.01 (mean \pm SD). No noticeable correlation between the spread of the data around the line and the intensity is observed. **(F)** Histogram of distance to the fitted line of each data point in (D). The average root-mean-square (RMS) distance with respect to the fitted line for the data set combinations is $(1.0 \pm 0.1) \times 10^3$ arbitrary fluorescence units (au) (mean \pm SD). **(G)** Relative error in fluorescence intensity as a function of the spot intensity. The absolute spot intensities are sorted into different percentiles and the error stemming from averaging (black) and from estimating the offset (red, see(D)) is computed. Error bars are standard deviations. From this plot we conclude that the uncertainty in determining the offset is higher than the uncertainty stemming from averaging multiple frames. When individual spot traces are plotted the error in estimating the background is used as a proxy for the total error in estimating the fluorescence. **(H)** Histogram of the minimum fluorescence per detected particle for all collected data ($n_{\text{particles}} \approx 5800$). Black line is a fit to a normal distribution to estimate a detection limit, which can be converted using the absolute calibration (Figure S3) to 6 ± 3 nascent mRNA molecules per fluorescent spot. **(I)** Systematic error associated with detecting dim spots in the posterior region of the boundary is determined by selecting the brightest peak plane DoG values observed throughout the life of each nucleus and plotting them in a histogram. The different plots indicate choices of the threshold applied on the shadow plane (32.5, 35 and 37.5 from left to right). Blue bars correspond to data taken in the posterior region, where the overall transcription signal is low. Red bars correspond to data taken in the anterior region. Magenta bars stem from data taken in the absence of the reporter construct. The left peak found in the distribution of posterior spots (blue) is associated with noise which can contribute to our count as false positives. This is justified by the fact that the left peak coincides with the control distribution obtained in the absence of reporter. The right peak of the blue distribution corresponds to real spots. In the case of the anterior distribution all spots detected are real spots due to the fact that every nucleus is turned on. As a result, no noise peak is noticeable in the histogram. In order to estimate the percentage of false positives and false negatives two Gaussians are fitted to the posterior distribution for different values of the shadow threshold. In each case the optimum threshold is determined by the intersection of the two Gaussian curves (dashed line located at 61.6, 58.9 and 41.6, respectively). The area under the Gaussian to the right of the threshold is used to estimate the fraction of false positives, and the fraction of false negatives is estimated from the area under the Gaussian to the left of the threshold (green shaded area) resulting in a systematic error for each threshold used of 5%, 4% and 10% from left to right. The clear separation between detected spots and noise fluorescence indicates that nuclei in which no spots are detected present no transcription or transcribe at levels that are significantly lower than our detection limit.

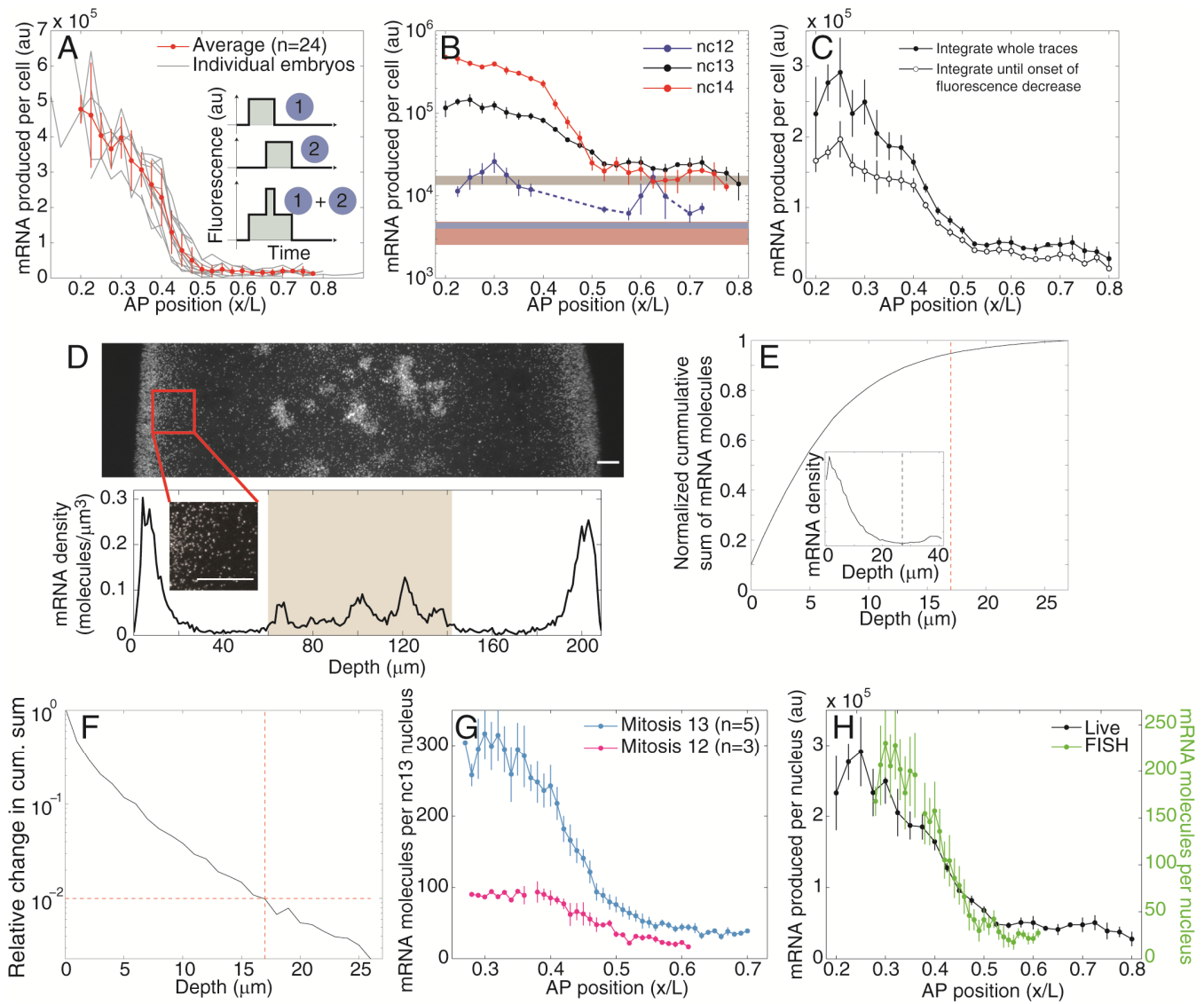


Figure S3. Inferring the absolute number of mRNA molecules accumulated, related to Figure 2. (A) (Inset: Each polymerase numbered as in Figure 1A will contribute to the overall fluorescence trace in an independent manner. The area under the fluorescence curve will be proportional to the total number of mRNA molecules produced). 24 profiles of the amount of mRNA produced as a function of AP (grey lines). Imaging window in individual embryos cover an AP range of ~20%EL. Full AP profile is obtained by averaging these profiles in 2.5%EL bins (red points). **(B)** Total amount of mRNA produced per n.c. 14-equivalent-cell (i.e. the production per cell in n.c.12 and n.c. 13 is divided by four and two, respectively, to compensate for nuclei associated cytoplasmic volume changes from n.c. to n.c.) as a function of AP position as in Figure 3A (note log scale on y-axis). Blue, gray and red horizontal bars correspond to the mean and standard error of the effective mRNA production in embryos carrying a *bcd*^{E1} mutation (Figure S5). **(C)** It is possible that not all PolII molecules contributing to the fluorescence result in a finished transcript. As a result, the calculation of the total amount of mRNA produced from the integral of fluorescent traces (Figure 3A) could be systematically overestimated. In particular, if the decrease in signal at the onset of fluorescent decay is due to mitotic repression [S16, 17], for example, none of the fluorescence past this time point should be considered. The systematic error in the integration is estimated by identifying the onset of mitotic repression with the promoter turn off time, t_{off} (Figure 3B). The overall number of mRNA molecules produced as a function of AP position shows a decrease with respect to integrating over the whole life of a spot of $(29 \pm 9)\%$. However, the dynamic range remains comparable with 5.8 ± 0.4 when integrating over the whole life time of spots and 5.8 ± 0.8 when only considering their traces until t_{off} . We conclude that the dynamic range is not sensitive to the window of time of integration. On the other hand, the absolute value obtained from integration is sensitive to the time window, setting a bound on the reliability of the comparison of absolute levels measured by live imaging and mRNA FISH. **(D)** Typical midsagittal section in the anterior region of an embryo (~35%EL location along the AP axis) carrying a version of our reporter construct without the MS2 stem loops (top). Individual cytoplasmic mRNA molecules are resolved (inset) [S9]. The distribution of mRNA molecules peaks at the surface of the embryo and decays towards the interior yolk region (bottom). At a position midway to the center of the embryo the production from yolk nuclei

(peaks between 60 μ m and 140 μ m, shaded area) is significant. Due to embryo deformation stemming from the protocol these distances vary from embryo to embryo. Therefore, the optimum depth in the apical-basal direction for counting all cytoplasmic transcripts was determined independently for each embryo. Scale bar is 10 μ m. **(E)** Cumulative cytoplasmic *lacZ*-mRNA distribution integrated from the embryo surface to the optimum depth as a function of apical-basal depth. Inset shows the distribution of mRNA molecules as a function of depth into the embryo from which the optimal depth is determined (dashed black line). **(F)** The relative change in the cumulative sum as a function of depth, used to find a depth at which the sum changes by less than 1% (red dashed lines). This distance corresponds to more than 90% of all mRNA molecules detected (red dashed line in (D)). **(G)** Cytoplasmic mRNA profiles during mitosis 12 and 13 (averages of $n=3$ and $n=5$ embryos, respectively) when mRNA production is shut down [S16, 17]. Given the stability of the 3'UTR of our reporter construct [S18] we interpret these profiles as indicating the total amount of accumulated mRNA until mitosis 12 and 13, respectively. **(H)** The total amount of mRNA produced during n.c. 13 is obtained by subtracting the profile for mitosis 12 from the profile for mitosis 13 reported in (D). The obtained FISH profile is overlaid with the total amount of mRNA produced in n.c. 13 inferred from the MS2 data by normalizing to the anterior region. This provides a calibration of the live profile with absolute mRNA counts, allowing for reports of the absolute amount of produced mRNA (Figure 3A). Since the systematic error in measuring absolute levels with the live imaging technique can be as high as 29% this calibration should only be viewed as an estimate. Using this result we determine the integrated fluorescence intensity corresponding to the transit of one polymerase molecule along the gene (A, inset). Dividing this intensity value by the time of elongation (Figure 3B) yields an average fluorescence per polymerase molecule. Consequently, we calibrate the fluorescent traces in terms of the absolute number of transcribing polymerases per fluorescent spot (Figures 1D and 3B,C). The dynamic range of the two profiles is comparable (FISH 7.3 ± 0.7 and MS2 5.8 ± 0.8). The systematically wider transition region obtained from live imaging is attributed to the fact that the profile is constructed by averaging multiple embryos spanning only 20%EL as opposed to mRNA FISH which allows for the imaging of the whole profile in single embryos. (C, error bars are standard deviations over multiple embryos; D,E,G,H error bars are standard errors over multiple embryos).

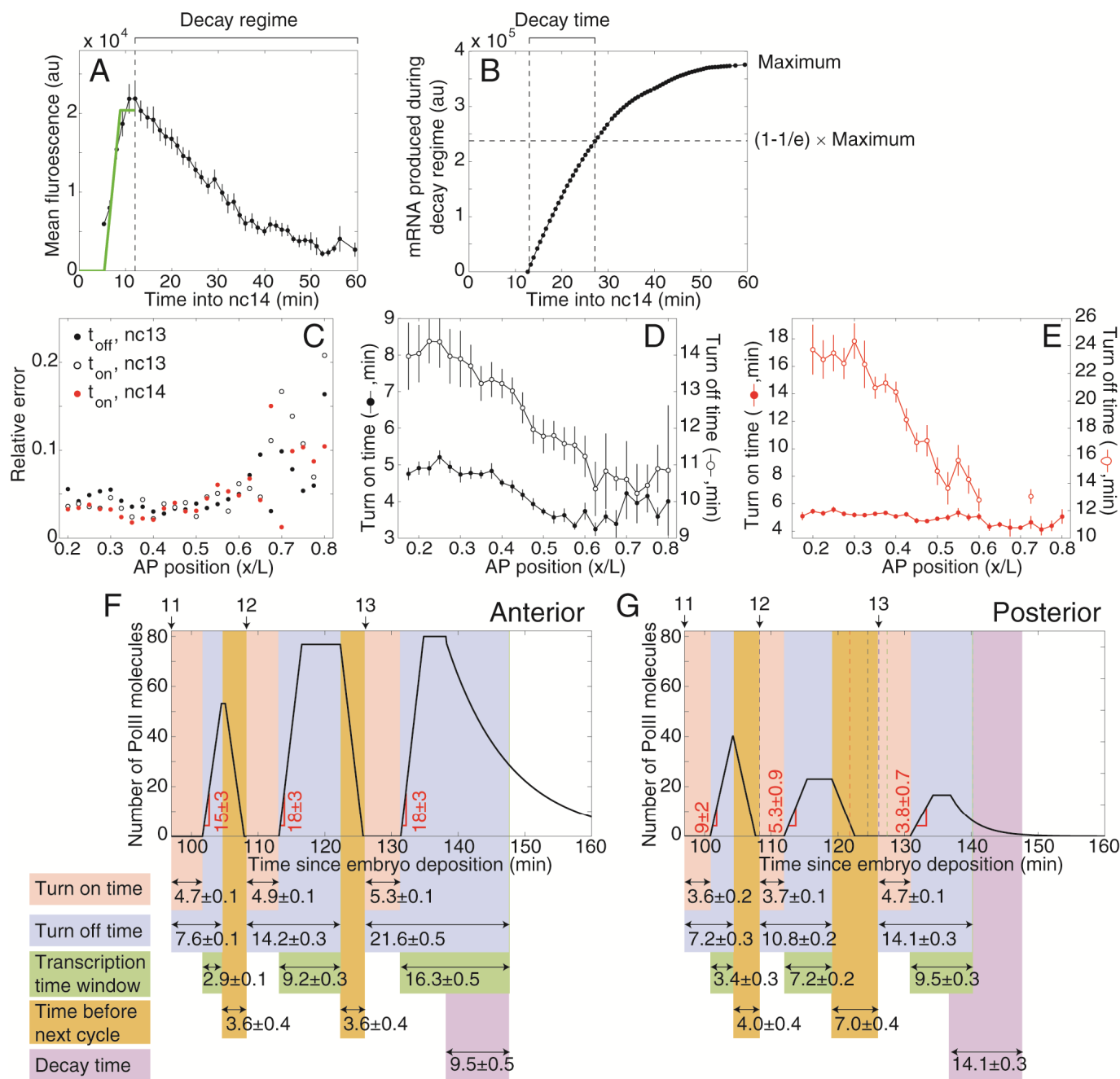


Figure S4. Extracting transcriptional dynamics using a simple model of regulation, related to Figure 3. (A) In n.c. 14 the first part of mean fluorescence as a function of time is fit using a model as described in the text (Figure 3B,C). The decay regime in n.c. 14 is defined from the point where the fluorescence starts decreasing (black dashed line) until the end of the trace (at 60 min). (B) The integral of the fluorescence in the decay regime corresponds to the amount of mRNA produced as a function of time (Figure S3A-C). The decay time is calculated by finding the time point at which the integrated signal is within $1/e$ of its maximum. This time is then used to calculate the time of transcription turn off, t_{off} . (C) As we move from anterior to posterior the detected spots have a smaller overall fluorescence, making it more difficult to discern them. As a result, the estimation of the time of promoter turn on and turn off will be affected. The plot shows the relative error of measurements of these turn-on and turn-off times as obtained by the fit to our model (Figure 3A,B) as a function of AP. For positions near the posterior end of the embryo the error in time determination can be as high as 20%. This error is small compared to the modulation of the time window in n.c. 14 of 1.9 ± 0.1 (Figure 4B). (D,E) Time of promoter turn on (solid circles) and turn off (open circles) in n.c. 13 (D) and n.c. 14 (E) as a function of position along the embryo. Both the promoter turn on and turn off times are modulated in n.c. 13. However, they do so by keeping their difference almost constant resulting in a small

modulation of the window of time of active transcription (Figure 4B). In n.c. 14 only the time of promoter turn off displays a strong a modulation along the AP axis.**(F,G)** For n.c. 12, 13 and 14 the rate of polymerase loading (RNAP molecules/min, shown in red) and the different times related to the transcription process (in min) per fluorescent spot are shown for the (F) anterior and (G) regions. We define the beginning of a n.c. as the onset of anaphase. Transcription begins approximately 5 min into a n.c. and ends 3.6 min before the next n.c. Although interphases 12 and 13 last about 10 and 13 min, respectively [S19], the time during which polymerase loading occurs in the anterior region is only (2.9 ± 0.1) min for n.c. 12 and (9.2 ± 0.3) min for n.c. 13. (All errors are standard errors of the mean).

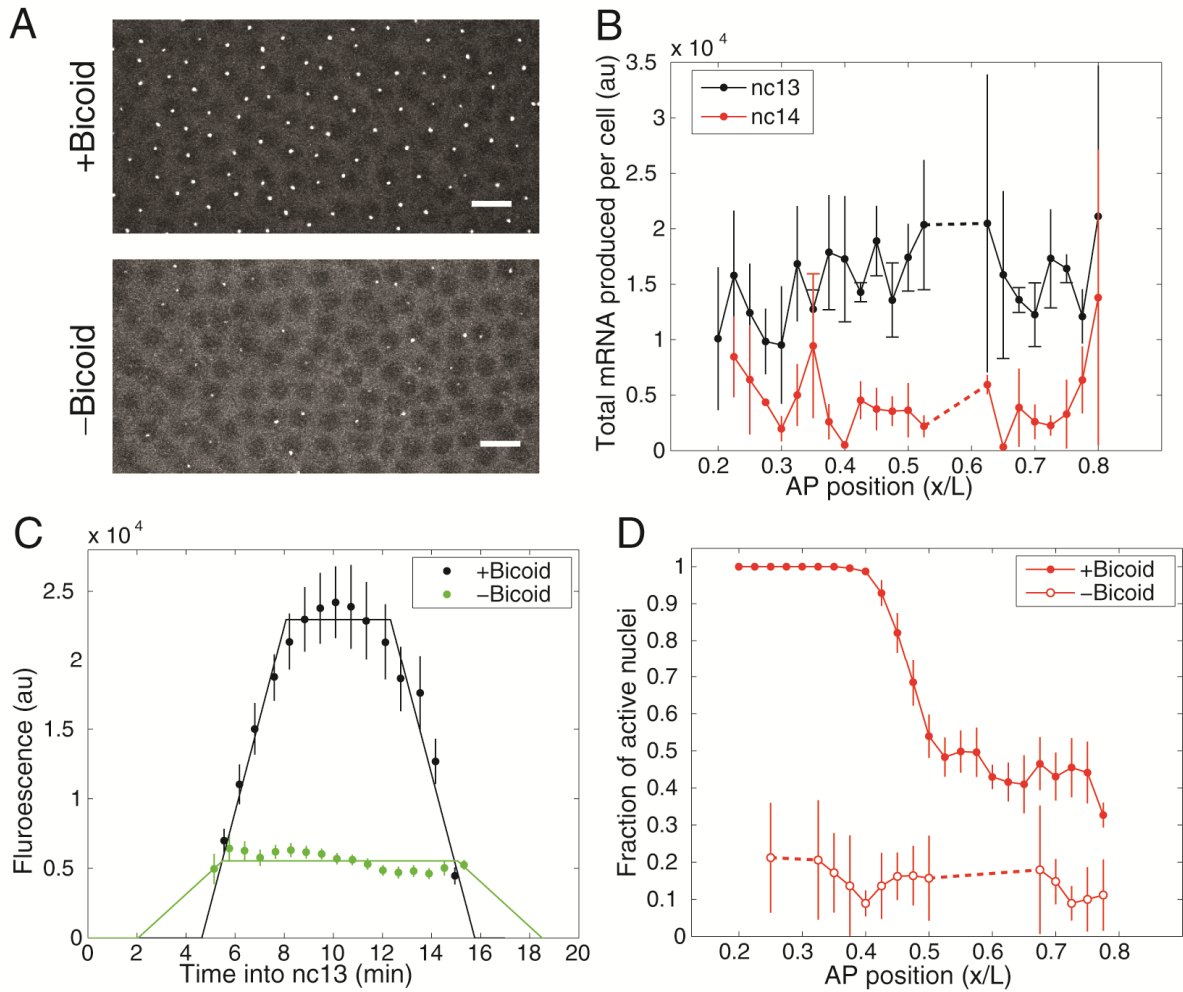


Figure S5. Basal transcriptional activity in the absence of Bcd, related to Figure 4. Throughout the embryo transcription sites are observed in the absence of the activator Bcd. **(A)** Comparison of a field of view in the anterior region in the presence (left) and absence (right) of Bcd activator in n.c. 13 (using the null mutant *bcd^{E1}*). Note that the brightness and contrast has been adjusted to make the presence of spots clear. Scale bar is 10 μm . **(B)** Total mRNA produced per n.c. 14 cell (i.e. the production per cell in n.c. 13 is divided by two) in the absence of Bcd for n.c. 13 (black) and n.c. 14 (red). The profiles show no clear dependence with AP position. The basal amount of mRNA produced by *bcd^{E1}* embryos is an order of magnitude lower than the amount produced in the anterior region in the presence of Bcd. **(C)** Average fluorescence of spots in wild-type (Ore-R) embryos (black, at 30% EL) and in *bcd^{E1}* mutant embryos (green, over the whole embryo) in n.c.13. The rate of transcription initiation of the *bcd^{E1}* mutant is obtained by fitting to our model (Figures 2B and 3B). **(D)** Fraction of active nuclei as a function of AP position in n.c. 14 in the presence of Bcd and in a *bcd^{E1}* mutant. Interestingly, the fraction of active nuclei at the posterior end, where vanishing concentrations of Bcd protein are present [S6], is $43 \pm 2\%$. However, in the absence of Bcd this number decreases to $15 \pm 2\%$, indicating a uniform Bcd-dependent change in overall capacity of nuclei to transcribe. We speculate on two possible molecular scenarios to explain this observation. First, the reporter construct could read out nuclear Bcd concentration in a non-equilibrium manner such that vanishing Bcd concentrations are distinguishable from not having Bcd at all. Second, a molecular species could be activated by a Bicoid-dependent process in the anterior region and diffuse throughout the embryo by n.c. 14, affecting the nuclear transcriptional capacity. (A, D, error bars are standard errors over multiple embryos; B, error bars are standard errors over multiple nuclei).

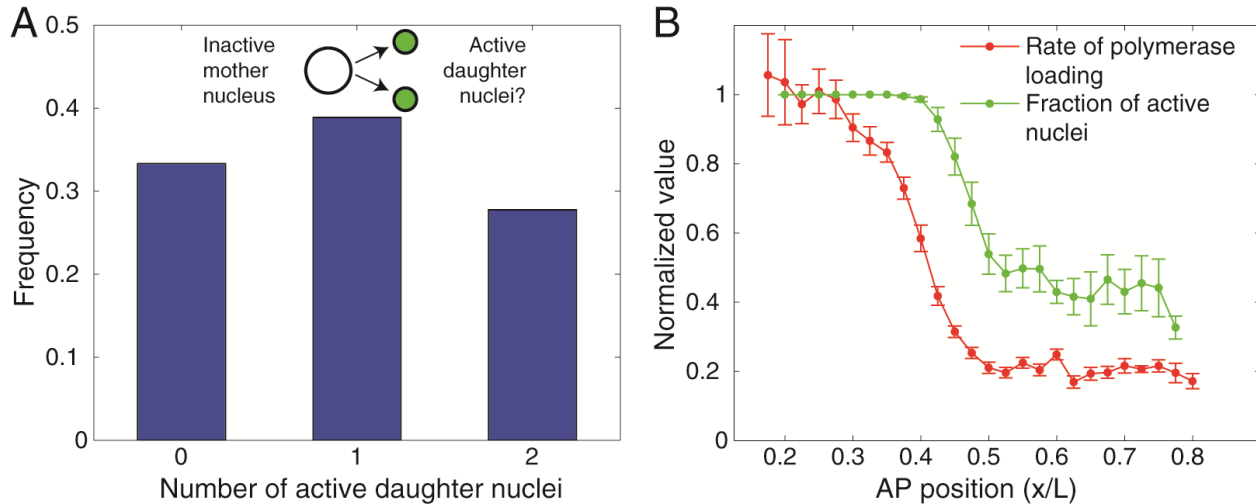


Figure S6. Control of the fraction of active nuclei, related to Figure 4. (A) Histogram of the number of active n.c. 14 daughter nuclei stemming from mother nuclei that were inactive ($n=18$). Nuclei that are inactive in n.c. 13 divide into daughter nuclei with no particular preference for activation in n.c. 14. This result suggests that the activity of a nucleus is stochastic and that the state of nuclear activity is not memorized. This observation contrasts with previous reports of a memory effect in the synchrony of early *hb* expression [S20]. (B) Rate of polymerase loading (red) and fraction of active nuclei (green) as a function of AP position. Data points are average and standard error over multiple embryos in AP bins of 2.5%. When arbitrarily normalizing the anterior region to 1 a clear boundary shift is detected. As a consequence, as one moves along the boundary from the anterior toward the posterior the rate of polymerase loading decreases while all nuclei are still active. Only when the rate of polymerase loading has decreased to ~50% of its peak value the modulation of the fraction of active nuclei becomes apparent. The fact that the two boundaries are not coinciding indicates that the two regulatory parameters are controlled in an independent fashion. As both parameters are Bcd dependent, it also indicates that the modulation of the fraction of activated nuclei is controlled by a loading-rate-independent interaction of Bcd with the P2 enhancer. This scenario can be realized if the rate of polymerase loading and the fraction of active nuclei are controlled by two different sets of binding sites on the P2 enhancer, each with a different dissociation constant. For instance, high affinity binding sites for Bcd could regulate chromatin accessibility, while lower affinity ones the rate of polymerase loading [S21, 22].

Supplemental References

- S1. van Gemert, A.M., van der Laan, A.M., Pilgram, G.S., Fradkin, L.G., Noordermeer, J.N., Tanke, H.J., and Jost, C.R. (2009). In vivo monitoring of mRNA movement in *Drosophila* body wall muscle cells reveals the presence of myofiber domains. *PLoS ONE* 4, e6663.
- S2. Chen, H., Xu, Z., Mei, C., Yu, D., and Small, S. (2012). A system of repressor gradients spatially organizes the boundaries of bicoid-dependent target genes. *Cell* 149, 618-629.
- S3. Bateman, J.R., Lee, A.M., and Wu, C.T. (2006). Site-specific transformation of *Drosophila* via phiC31 integrase-mediated cassette exchange. *Genetics* 173, 769-777.
- S4. Gregor, T., Wieschaus, E.F., McGregor, A.P., Bialek, W., and Tank, D.W. (2007). Stability and nuclear dynamics of the bicoid morphogen gradient. *Cell* 130, 141-152.
- S5. Di Talia, S., and Wieschaus, E.F. (2012). Short-term integration of Cdc25 dynamics controls mitotic entry during *Drosophila* gastrulation. *Developmental cell* 22, 763-774.
- S6. Liu, F., Morrison, A.H., and Gregor, T. (2013). Dynamic interpretation of maternal inputs by the *Drosophila* segmentation gene network. *Proc Natl Acad Sci U S A* 110, 6724-6729.
- S7. Idema, T. (2013). A new way of tracking motion, shape, and divisions. *European biophysics journal : EBJ*.
- S8. Young, J.W., Locke, J.C., Altinok, A., Rosenfeld, N., Bacarian, T., Swain, P.S., Mjolsness, E., and Elowitz, M.B. (2012). Measuring single-cell gene expression dynamics in bacteria using fluorescence time-lapse microscopy. *Nat Protoc* 7, 80-88.
- S9. Little, S.C., Tikhonov, M., and Gregor, T. (2013). Precise developmental gene expression arises from globally stochastic transcriptional activity. *Cell in press*.
- S10. Little, S.C., Tkacik, G., Kneeland, T.B., Wieschaus, E.F., and Gregor, T. (2011). The formation of the Bicoid morphogen gradient requires protein movement from anteriorly localized mRNA. *PLoS Biol* 9, e1000596.
- S11. Rosenfeld, N., Young, J.W., Alon, U., Swain, P.S., and Elowitz, M.B. (2005). Gene regulation at the single-cell level. *Science* 307, 1962-1965.
- S12. Kuhlman, T., Zhang, Z., Saier Jr., M.H., and Hwa, T. (2007). Combinatorial transcriptional control of the lactose operon of *Escherichia coli*. *Proc Natl Acad Sci U S A* 104, 6043-6048.
- S13. Bintu, L., Buchler, N.E., Garcia, H.G., Gerland, U., Hwa, T., Kondev, J., Kuhlman, T., and Phillips, R. (2005). Transcriptional regulation by the numbers: applications. *Curr Opin Genet Dev* 15, 125-135.
- S14. Jaeger, J., Surkova, S., Blagov, M., Janssens, H., Kosman, D., Kozlov, K.N., Manu, Myasnikova, E., Vanario-Alonso, C.E., Samsonova, M., et al. (2004). Dynamic control of positional information in the early *Drosophila* embryo. *Nature* 430, 368-371.
- S15. Wilkie, G.S., Shermoen, A.W., O'Farrell, P.H., and Davis, I. (1999). Transcribed genes are localized according to chromosomal position within polarized *Drosophila* embryonic nuclei. *Curr Biol* 9, 1263-1266.
- S16. Shermoen, A.W., and O'Farrell, P.H. (1991). Progression of the cell cycle through mitosis leads to abortion of nascent transcripts. *Cell* 67, 303-310.
- S17. Rothe, M., Pehl, M., Taubert, H., and Jackle, H. (1992). Loss of gene function through rapid mitotic cycles in the *Drosophila* embryo. *Nature* 359, 156-159.
- S18. Thomsen, S., Anders, S., Janga, S.C., Huber, W., and Alonso, C.R. (2010). Genome-wide analysis of mRNA decay patterns during early *Drosophila* development. *Genome Biol* 11, R93.
- S19. Foe, V.E., Odell, G.M., and Edgar, B.E. (1993). Mitosis and morphogenesis in the *Drosophila* embryo: Point and counterpoint. In *The Development of Drosophila melanogaster*, M. Bate and A. Martinez Arias, eds. (Plainview, N.Y.: Cold Spring Harbor Laboratory Press).
- S20. Porcher, A., Abu-Arish, A., Huart, S., Roelens, B., Fradin, C., and Dostatni, N. (2010). The time to measure positional information: maternal hunchback is required for the synchrony of the Bicoid transcriptional response at the onset of zygotic transcription. *Development* 137, 2795-2804.
- S21. Mirny, L.A. (2010). Nucleosome-mediated cooperativity between transcription factors. *Proc Natl Acad Sci U S A* 107, 22534-22539.
- S22. Lam, F.H., Steger, D.J., and O'Shea, E.K. (2008). Chromatin decouples promoter threshold from dynamic range. *Nature* 453, 246-250.